Electronic Supplementary Material (ESI) for RSC Advances.

Supporting Information

Controlled Assembly of Cobalt embedded N-doped Graphene Nanosheets (Co@NGr) Derived by Pyrolysis of Mixed Ligand Co(II) MOF as a Sacrificial Template for High-Performance Electrocatalyst

Gopala Ram Bhadu,[a]* Bhavesh Parmar,[a] Parth Patel,[b,c] Jayesh C. Chaudhari,[a] and Eringathodi Suresh[a,d]*

[a]Analytical and Environmental Science Division and Centralized Instrument Facility, CSIR–Central Salt and Marine Chemicals Research Institute, G. B. Marg, Bhavnagar-364 002, Gujarat, India.

[b]Inorganic Materials and Catalysis Division, CSIR-Central Salt and Marine Chemicals Research Institute, G. B. Marg, Bhavnagar-364 002, Gujarat, India.

[c]Charotar University of Science & Technology, Changa-388 421, Anand, Gujarat, India.

[d]Academy of Scientific and Innovative Research (AcSIR), Ghaziabad-201 002, India.

E-mail: grbhadu@csmcri.res.in; esuresh@csmcri.res.in; sureshe123@rediffmail.com

Experimental Section

Materials and General Methods: All reagents and solvents were purchased from commercial sources and were used without further purification. Milli-Q water was used for synthetic manipulations. FT-Raman data were collected using a Horiba Scientific LabRAM HR Evolution Raman Spectrometer with 532 nm line of an Ar ion laser at room temperature. Powder X-ray diffraction (PXRD) data were collected using a PANalytical Empyrean (PIXcel 3D detector) system with CuK_{α} radiation. N_2 adsorption-desorption isotherm and BET surface area was measured on a Micromeritics, 3 Flex instrument. Field Emission-Scanning Electron Microscopy (FE-SEM) micrographs were recorded using a JEOL JSM-7100F instrument employing an 15-kV accelerating

voltage. Transmission electron microscopy (TEM) images were recorded on a JEOL JEM-2100 microscope with an acceleration voltage of 200 kV using lacey carbon-coated 300-mesh copper grids. X-ray photoelectron spectroscopy (XPS) analysis was carried out on a Thermo Fisher Scientific ESCALAB Xi+ instrument.

Synthesis of CoMOF-2: Bulk powder of **CoMOF-2** was synthesized *via* RT Stirring method according to our previous report.[S1] 10 mmol of $Co(NO_3)_2.6H_2O$, 10 mmol 1,4-benzenedicarboxylic acid (H_2**BDC**), 20 mmol NaOH and 10 mmol (*E*)-N'-(pyridin-4-ylmethylene) isonicotinohydrazide (**L**) in 100 mL H_2O:MeOH:EtOH (5:4:1/v:v) solvent were stirred in a 200 mL round bottom flask at room temperature for 8 h. The resulting precipitate was filtered and washed with H_2O:MeOH (1:1/v:v) followed by acetone and then air dried. Yield *ca.* 90 %.

Synthesis of Co@NGr nanomaterials: 1.5 gm of **CoMOF-2** was placed in a tube furnace and pyrolyzed at set temperature (700, 800, 900 ^oC) for 5 hr under N_2 gas condition at a heating rate of 5 ^oC min^{-1}. After completion of pyrolysis, furnace was cooled to room temperature and the collected electrocatalysts material at the respective temperature is labeled as Co@NGr-**700**, Co@NGr-**800** and Co@NGr-**900** respectively and thoroughly characterized.

Electrochemical Measurements

Materials and General Methods: All the electrochemical activity/measurements, *i.e.*, Oxygen Evolution Reaction (OER), Hydrogen Evolution Reaction (HER), Cyclic Voltammetry (CV), of the synthesized materials were performed by using Metrohm Autolab PGSTAT204 potentiostat/galvanostat electrochemical workstation under room temperature and ambient atmospheric pressure. The electrochemical impedance spectroscopy measurements were

carried out using Princeton applied research potentiostat-galvanostat (PARSTAT 2273) by the three-electrode system. For the measurements, the Glassy carbon electrode (GCE) of 3 mm diameter was used as a working electrode while Pt foil and Ag/AgCl (saturated KCl) were used as a counter and reference electrodes, respectively.

Electrode Preparation: To prepare a working electrode, GCE was mirror polished on nylon pad using alumina powder (0.3 µ) and washed with milli-Q (MQ) water. The polished and washed GCE was then ultrasonicated into 1:1 acetone and water mixture for 30 minutes and dried properly at room temperature. A fixed amount of 5 mg electrocatalyst material was dispersed in 1 ml isopropanol (IPA) solvent and 10 µl Nafion was mixed separately with 90 µl MQ water. Both the solutions were separately ultrasonicated for 30 minutes. After proper dispersion, 10 µl was taken from each solution and mixed together in a separate vial and ultrasonicated for 30 min to form a homogenous ink. 10 µl of the completely dispersed catalyst ink was then loaded over the cleaned and dried surface of the bare GCE through drop-casting and kept overnight at 25 ^{o}C for drying. 1M KOH and 0.5M H_2SO_4 solutions were used as electrolytes for OER and HER process, respectively. Linear sweep voltammetry (LSV) was performed at 5mV/s scan rate in the potential range of 0.0 V to +2.0 V and 0.1 V to -1.2 V for the OER and HER process, respectively. Cyclic voltammetry was recorded from 0.0 V to +2.0 V potential at the scan rate of 25 mV/S to see the stability of the catalyst. Electrochemical impedance spectroscopy (EIS) was carried out in 1M KOH at the frequency range of 50 kHz to 100 mHz. The electrochemical active surface area (EASA) of the electrocatalyst was calculated from the curves which were obtained after performing cyclic voltammetry (CV) at different scan rates, *i.e.*, 1, 2, 3, 4, and 5 mV/s.

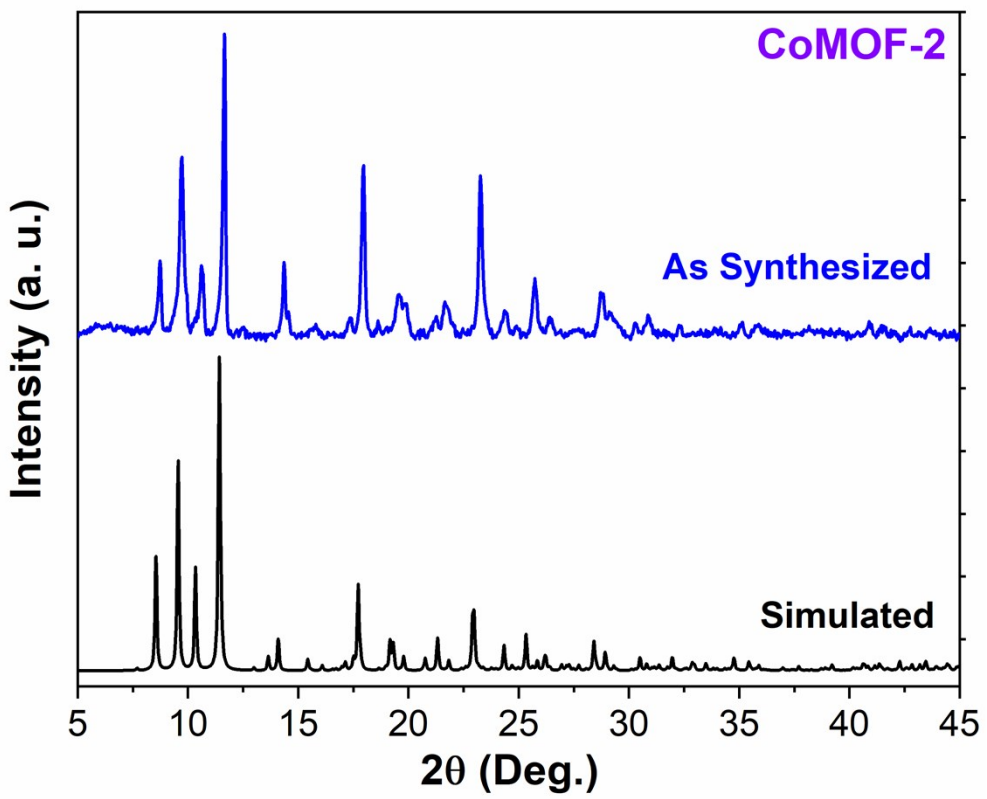

Figure S1. Comparison of PXRD data of **CoMOF-2** synthesized by RT stirring with simulated SXRD.

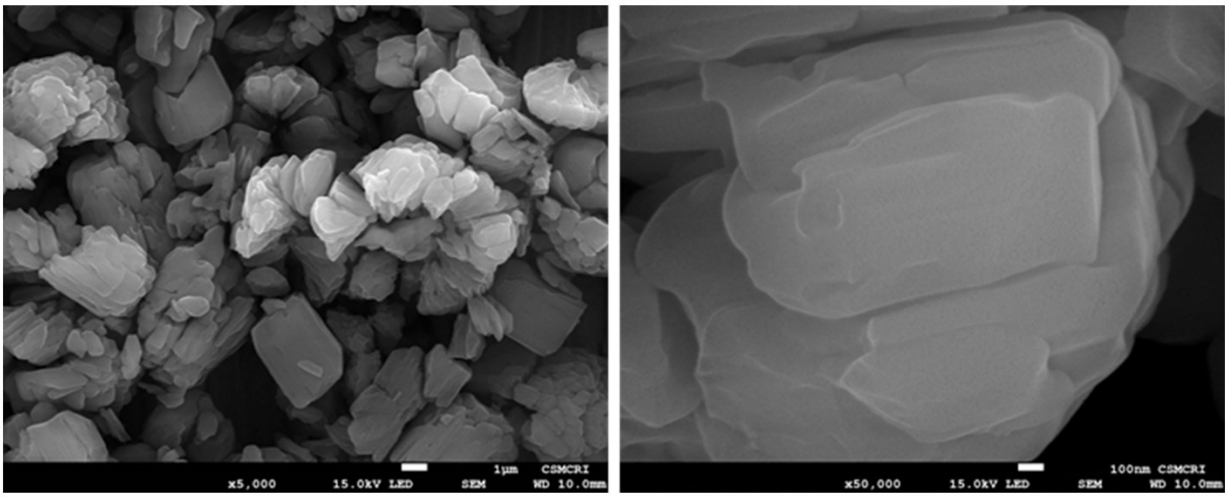

Figure S2. FE-SEM images recorded for **CoMOF-2** synthesized by RT stirring.

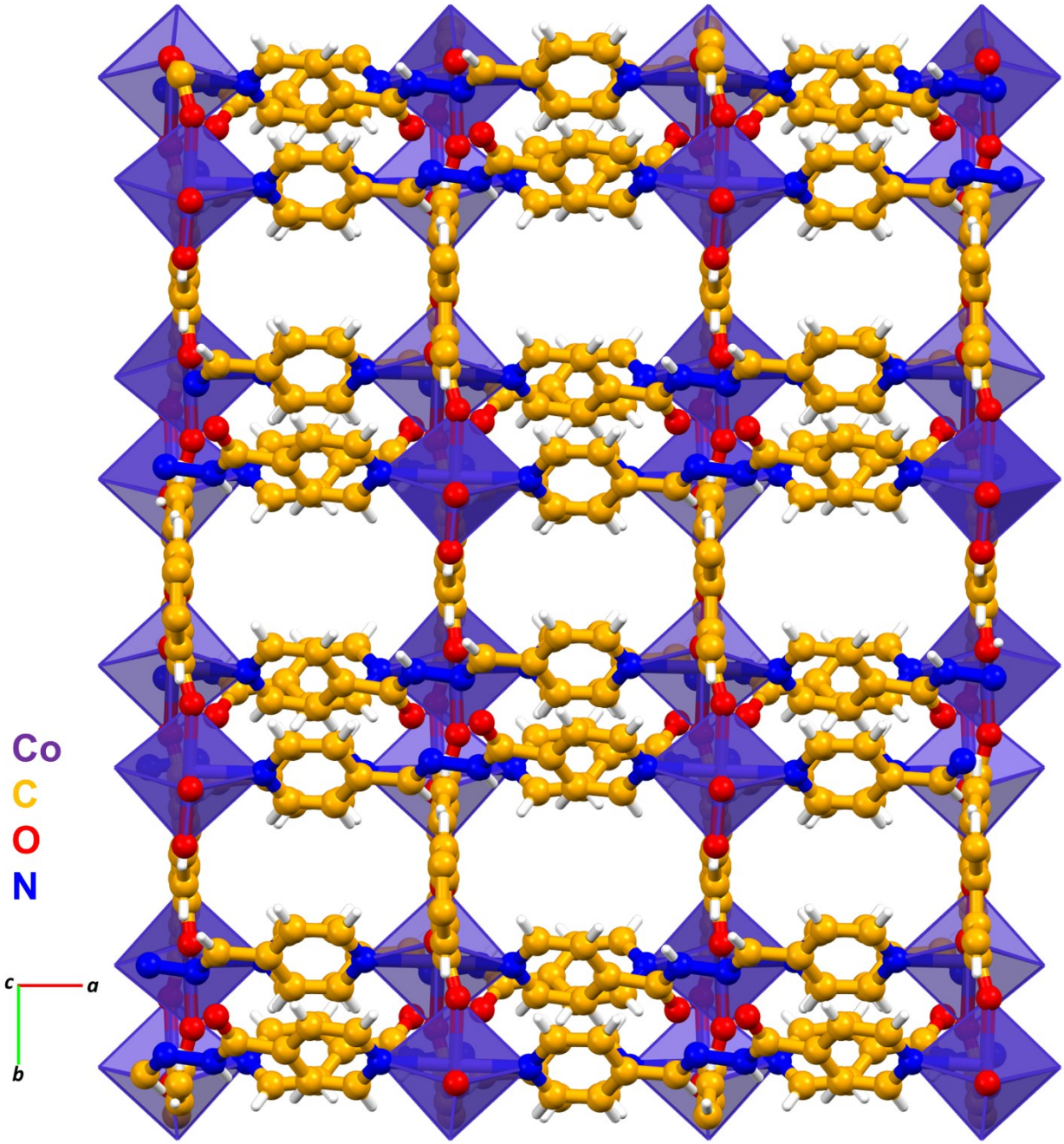

Figure S3. 3D framework in **CoMOF-2**, viewed down the *c*-axis.

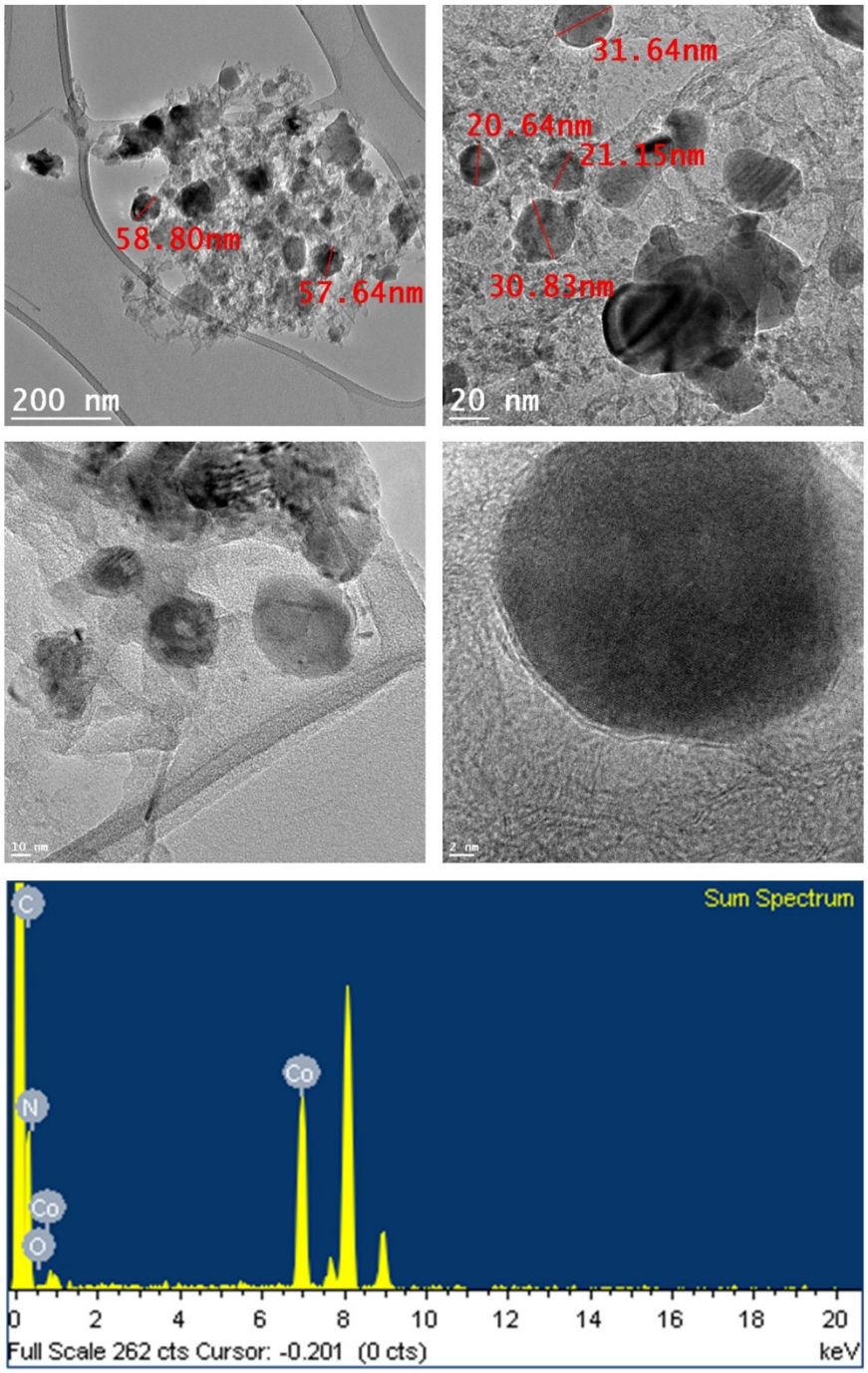

Figure S4. TEM images, HR-TEM images, SAED and TEM-EDX pattern of Co@NGr-**700**.

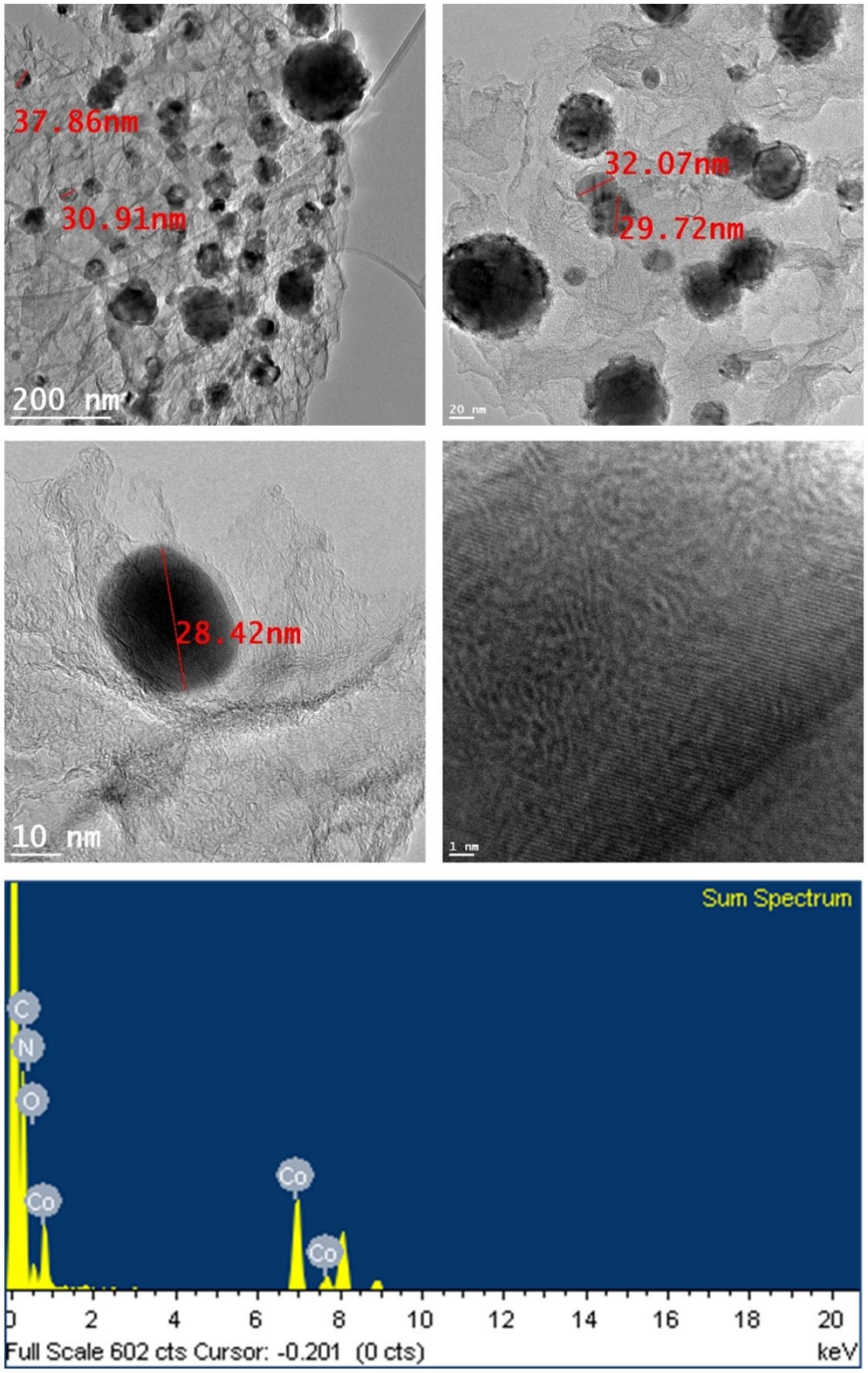

Figure S5. TEM images, HR-TEM images, SAED and TEM-EDX pattern of Co@NGr-**800**.

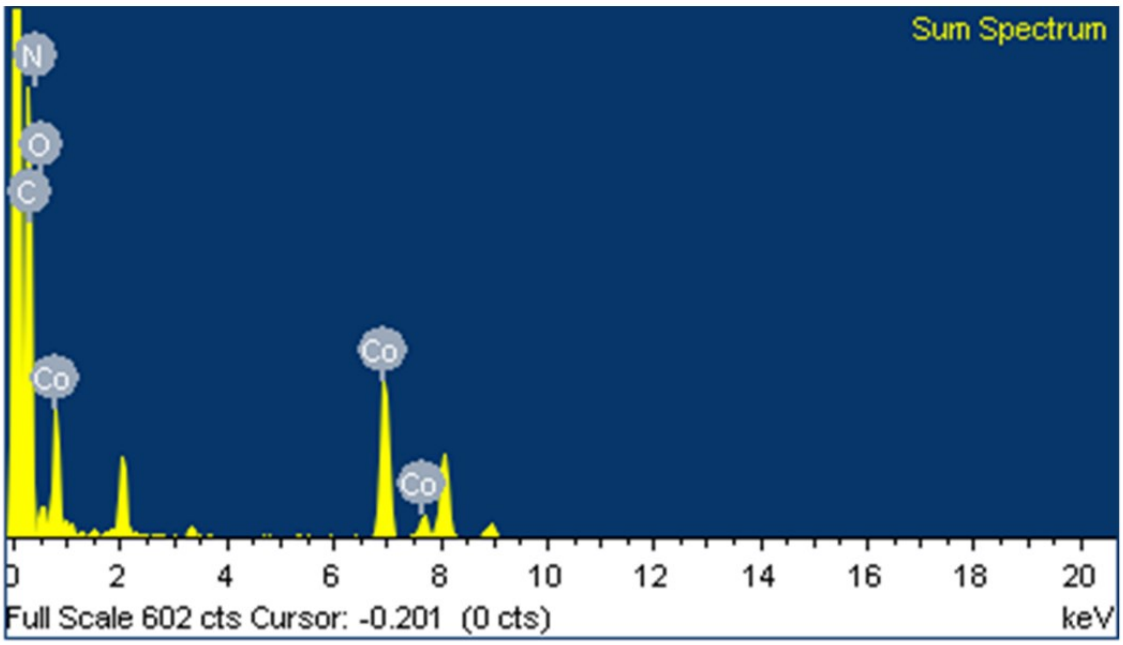

Figure S6. TEM-EDX pattern of Co@NGr-**900**.

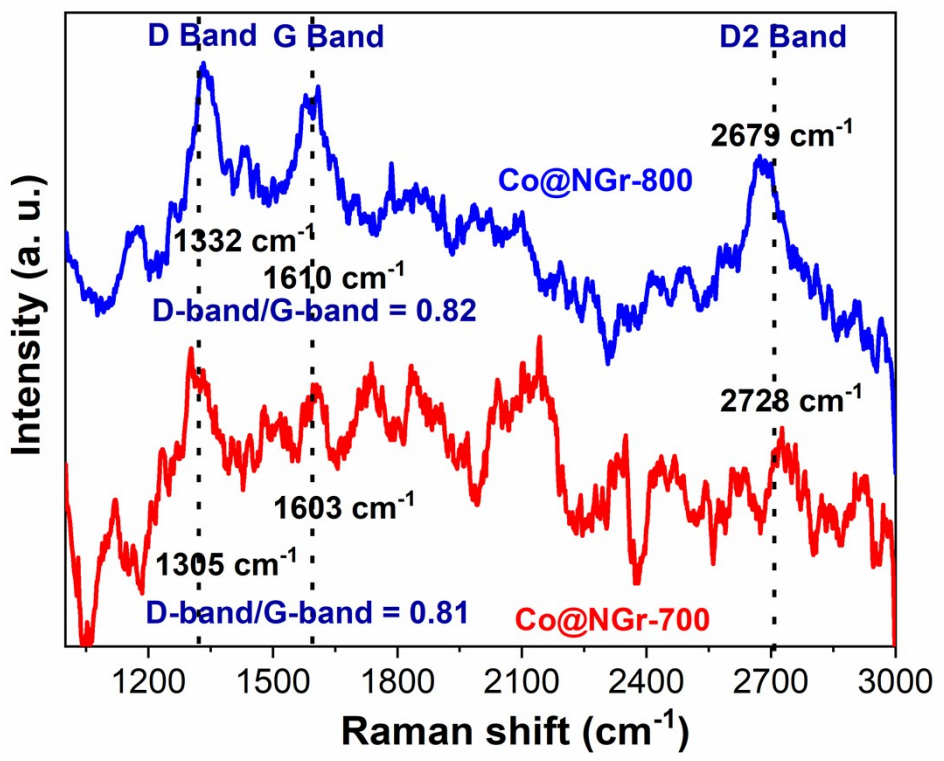

Figure S7. FT-Raman shift for Co@NGr-**700** and Co@NGr-**800**.

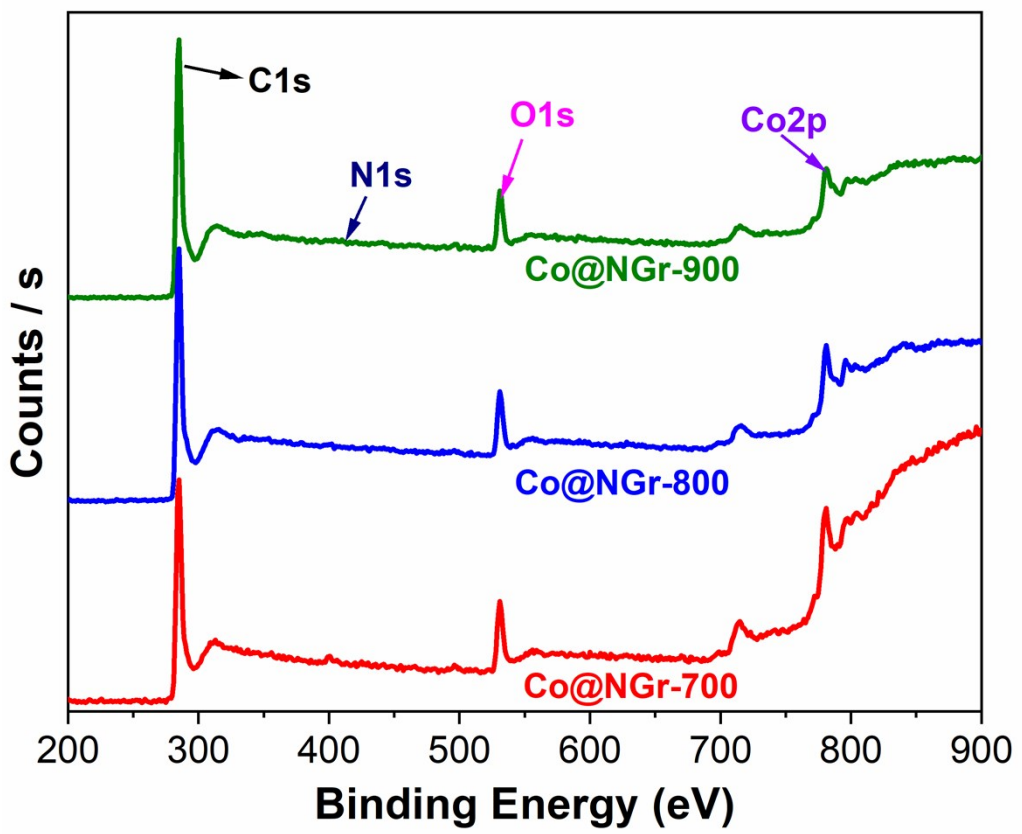

Figure S8. XPS survey spectrum of Co@NGr-**700**, Co@NGr-**800** and Co@NGr-**900** shows the peaks of C, N, O, and Co elements.

Table S1. Elemental composition of Co@NGr nanomaterials calcined at different temperature obtained from XPS analysis.

	XPS		
	Co@NGr-700	**Co@NGr-800**	**Co@NGr-900**
Co	6.3	5.5	4.03
C	80.27	84.94	87.21
N	3.27	0.75	0.69
O	10.15	8.8	8.07

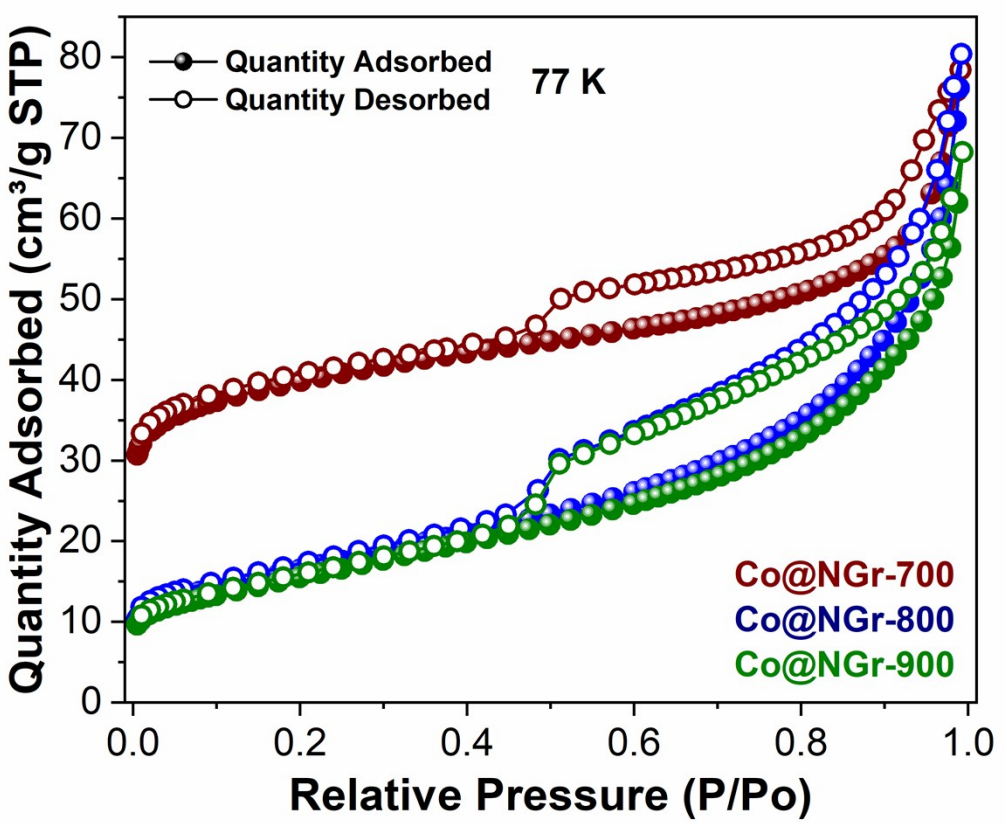

Figure S9. N_2 adsorption isotherm of Co@NGr-**700**/**800**/**900** nanomaterials at 77 K.

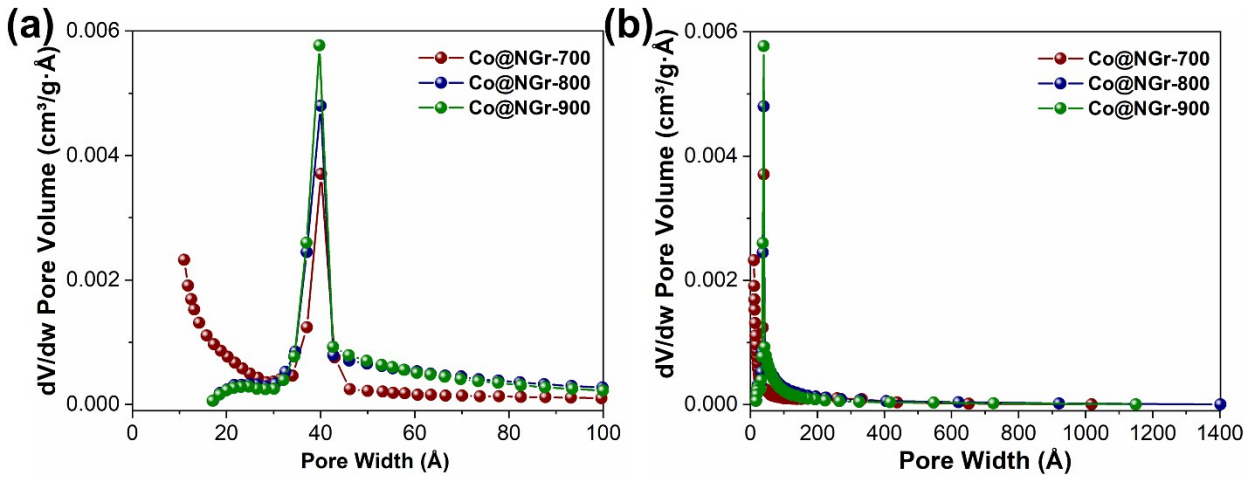

Figure S10. (a,b) BJH Desorption dV/dD Pore Volume plot for the mesopore determination in Co@NGr-**600**/**700**/**900** nanomaterials.

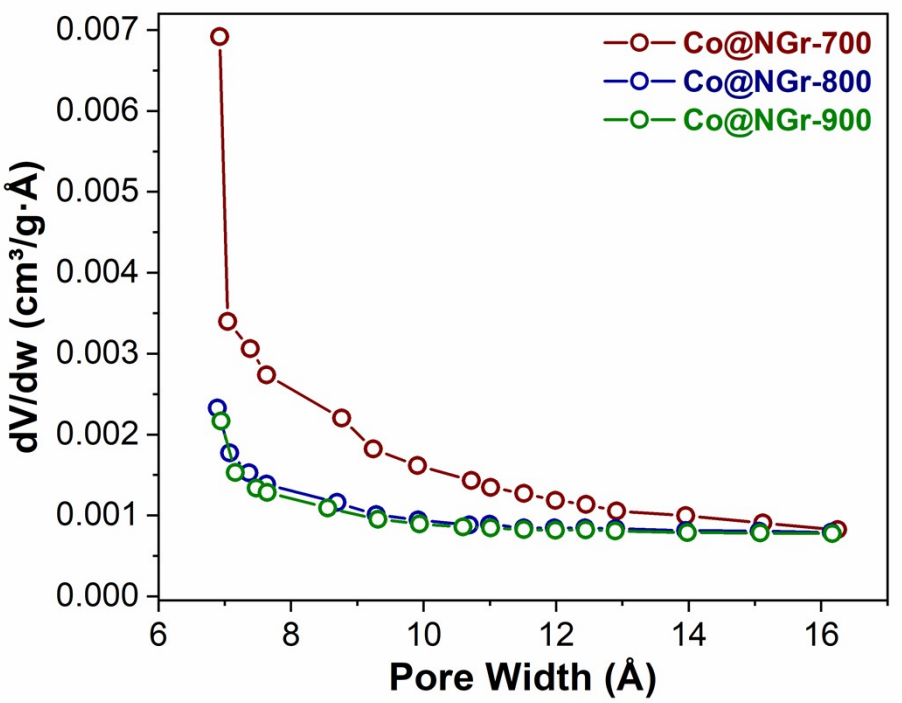

Figure S11. Horvath-Kawazoe Differential Pore Volume Plot for the micropore size determination in Co@NGr-**700**/**800**/**900** nanomaterials.

Table S2. Summary of BET surface area, average pore diameter and micropore size obtained from N_2 adsorption for Co@NGr-**700**/**800**/**900** nanomaterials.

	BET Surface Area (m^2/g)	Average Pore Diameter (Å)	Micropore Size (Å)
Co@NGr-**700**	127.4	38	6.92
Co@NGr-**800**	58.2	86	6.89
Co@NGr-**900**	54.9	77	6.94

Table S3. Summary of overpotential to achieve current density of 50 mA/cm^2 in OER and -50 mA/cm^2 in HER for different Co@NGr nanomaterials.

Co@NGr nanomaterials	Overpotential (mV) for OER at 10 mA/cm^2	Overpotential (mV) for HER at -10 mA/cm^2
Co@NGr-**700**	700	908
Co@NGr-**800**	590	625
Co@NGr-**900**	**520**	**628**

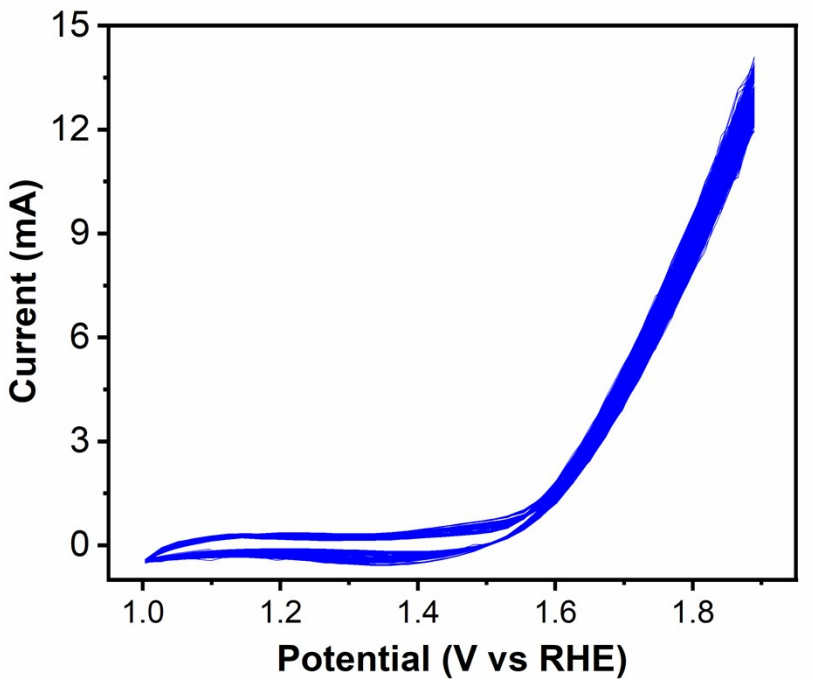

Figure S12. Cyclic voltammetry (CV) performed up to 200 cycles at 5 mV/s for Co@NGr-**900**.

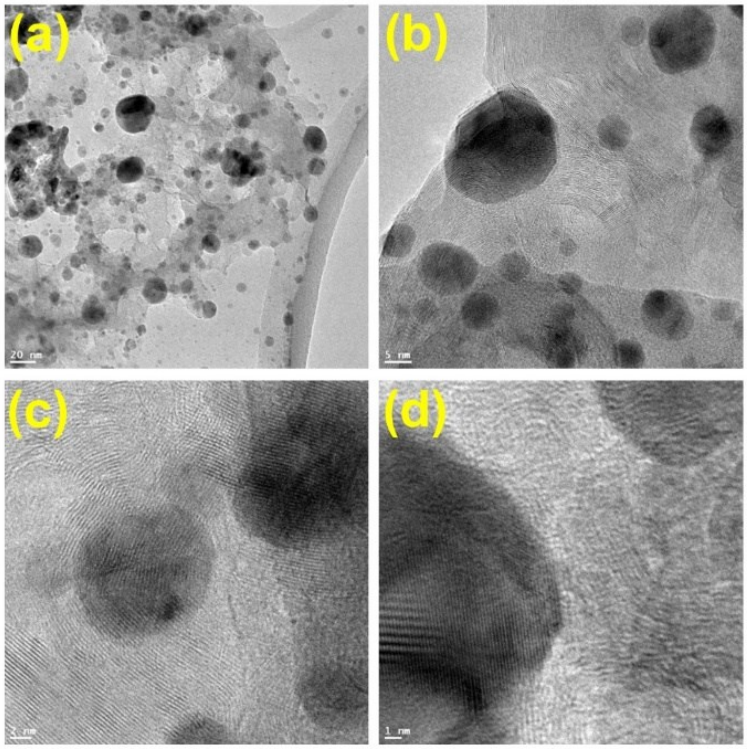

Figure S13. TEM images and HR-TEM images of recycled Co@NGr-**900**.

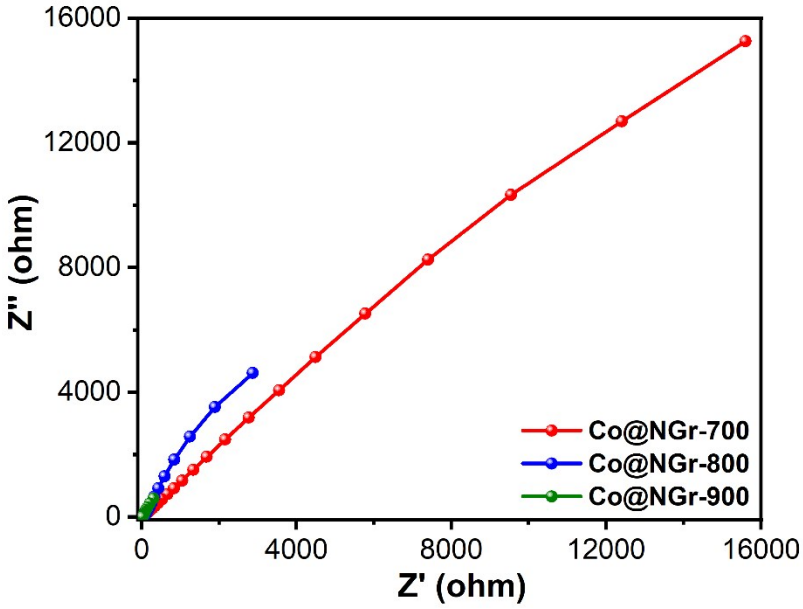

Figure S14. Nyquist Plot for Co@NGr-**700**/**800**/**900** nanomaterials.

Table S4. Comparison of the oxygen evolution reaction (OER) activities of recently reported electrocatalysts in respect of overpotential@10 mA/cm^2.

Sr No.	OER Electrocatalysts	Electrolytes	Overpotential@10 mA/cm^2 (mV)	Ref.
1	CoMOF-1@**900**	1 M KOH	210	S2
2	Co_3O_4/N-rmGO	1 M KOH	310	S3
3	Ultrathin $CoSe_2$ nanosheets	0.1 M KOH	320	S4
4	Annealed C−Co NPs	0.1 M KOH	390	S5
5	CoP/C	0.1 M KOH	360	S6
6	Co_2B-500/NG	0.1 M KOH	380	S7
7	CoP/rGO-400 (MOF-derived)	1 M KOH	340	S8
8	NCNTFs obtained at 700 ◦C (MOF-derived)	0.1 M KOH	370	S9
9	PNC/Co (MOF-derived)	1 M KOH	370	S10
10	Co-NC/CNT (MOF-derived)	1 M KOH	354	S11
11	Co@NCNT (MOF-derived)	1 M KOH	429	S12
12	CoZn-NC-700 (MOF-derived)	0.1 M KOH	390	S13
13	Co-N-CNTs (MOF-derived)	0.1 M KOH	460	S14
14	GNCNTs-4 (MOF-derived)	0.1 M KOH	370	S15
15	Co@N-CNTF-2 (MOF-derived)	1 M KOH	350	S16
16	Pt-SCFP/C-12	0.1 M KOH	370	S17
17	Co@NGr-**900**	1 M KOH	**390**	**This Work**

Table S5. Comparison of the hydrogen evolution reaction (HER) activities of recently reported electrocatalysts in respect of overpotential@-10 mA/cm^2.

Sr No.	HER Electrocatalysts	Electrolytes	Overpotential@-10 mA/cm^2 (mV)	Ref.
1	Co@N-CNTF-2 (MOF-derived)	0.5 M H_2SO_4	220	S16
2	NENU-500	0.5 M H_2SO_4	237	S18
3	NENU-501	0.5 M H_2SO_4	397	S18
4	Co@N–C-600	0.5 M H_2SO_4	339	S19
5	Co@NCNTs-800	0.5 M H_2SO_4	280	S20
6	CTGU-5	0.5 M H_2SO_4	388	S21
7	CTGU-6	0.5 M H_2SO_4	425	S21
8	THAT-Co	0.5 M H_2SO_4	283	S22
9	S-600	0.5 M H_2SO_4	262	S23
10	Ni_2P polyhedron	0.5 M H_2SO_4	158	S24
11	CoP NRAs	0.5 M H_2SO_4	181	S25
12	$NiMo_2C$@C	0.5 M H_2SO_4	169	S26
13	Fe_xP@NPC	0.5 M H_2SO_4	227	S27
14	CoMOF-1@**900**	0.5 M H_2SO_4	580	S2
15	Co@NGr-**900**	0.5 M H_2SO_4	**340**	**This work**

References:

S1 B. Parmar, P. Patel, R. S. Pillai, R. K. Tak, R. I. Kureshy, N. H. Khan and E. Suresh, Cycloaddition of CO_2 with an Epoxide-Bearing Oxindole Scaffold by a Metal–Organic Framework-Based Heterogeneous Catalyst under Ambient Conditions, *Inorg. Chem*., 2019, **58**, 10084-10096.

S2 G. R. Bhadu, B. Parmar, P. Patel, A. Paul, J. C. Chaudhari, D. N. Srivastava and E. Suresh, Co@N-doped carbon nanomaterial derived by simple pyrolysis of mixed-ligand MOF as an active and stable oxygen evolution electrocatalyst, *Appl. Surf. Sci.,* 2020, **529**, 147081.

S3 Y. Liang, Y. Li, H. Wang, J. Zhou, J. Wang, T. Regier and H. Dai, Co_3O_4 nanocrystals on graphene as a synergistic catalyst for oxygen reduction reaction, *Nat. Mater.,* 2011, **10**, 780-786.

S4 Y. Liu, H. Cheng, M. Lyu, S. Fan, Q. Liu, W. Zhang, Y. Zhi, C. Wang, C. Xiao, S. Wei, B. Ye and Y. Xie, Low Overpotential in Vacancy-Rich Ultrathin $CoSe_2$ Nanosheets for Water Oxidation, *J. Am. Chem. Soc.,* 2014, **136**, 15670-15675.

S5 L. Wu, Q. Li, C. H. Wu, H. Zhu, A. Mendoza-Garcia, B. Shen, J. Guo and S. Sun, Stable Cobalt Nanoparticles and Their Monolayer Array as an Efficient Electrocatalyst for Oxygen Evolution Reaction, *J. Am. Chem. Soc.,* 2015, **137**, 7071-7074.

S6 J. Chang, Y. Xiao, M. Xiao, J. Ge, C. Liu and W. Xing, Surface Oxidized Cobalt-Phosphide Nanorods As an Advanced Oxygen Evolution Catalyst in Alkaline Solution, *ACS Catal.,* 2015, **5**, 6874-6878.

S7 J. Ryu, N. Jung, J. H. Jang, H. -J. Kim and S. J. Yoo, In Situ Transformation of Hydrogen-Evolving CoP Nanoparticles: Toward Efficient Oxygen Evolution Catalysts Bearing Dispersed Morphologies with Co-oxo/hydroxo Molecular Units, *ACS Catal.,* 2015, **5**, 4066-4074.

S8 L. Jiao, Y. -X. Zhou and H. -L. Jiang, Metal–organic framework-based CoP/reduced graphene oxide: high-performance bifunctional electrocatalyst for overall water splitting, *Chem. Sci.,* 2016, **7**, 1690-1695.

S9 B. Y. Xia, Y. Yan, N. Li, H. B. Wu, X. W. Lou and X. Wang, A metal–organic framework-derived bifunctional oxygen electrocatalyst, *Nat. Energy,* 2016, **1**, 15006.

S10 X. Li, Z. Niu, J. Jiang and L. Ai, Cobalt nanoparticles embedded in porous N-rich carbon as an efficient bifunctional electrocatalyst for water splitting, *J. Mater. Chem. A,* 2016, **4**, 3204-3209.

S11 F. Yang, P. Zhao, X. Hua, W. Luo, G. Cheng, W. Xing and S. Chen, A cobalt-based hybrid electrocatalyst derived from a carbon nanotube inserted metal–organic framework for efficient water-splitting, *J. Mater. Chem. A,* 2016, **4**, 16057-16063.

S12 E. Zhang, Y. Xie, S. Ci, J. Jia, P. Cai, L. Yi and Z. Wen, Multifunctional high-activity and robust electrocatalyst derived from metal–organic frameworks, *J. Mater. Chem. A,* 2016, **4**, 17288-17298.

S13 B. Chen, X. He, F. Yin, H. Wang, D. -J. Liu, R. Shi, J. Chen and H. Yin, MO-Co@N-Doped Carbon (M = Zn or Co): Vital Roles of Inactive Zn and Highly Efficient Activity toward Oxygen Reduction/Evolution Reactions for Rechargeable Zn–Air Battery, *Adv. Funct. Mater.,* 2017, **27**, 1700795.

S14 T. Wang, Z. Kou, S. Mu, J. Liu, D. He, I. S. Amiinu, W. Meng, K. Zhou, Z. Luo, S. Chaemchuen and F. Verpoort, 2D Dual-Metal Zeolitic-Imidazolate-Framework-(ZIF)-Derived Bifunctional Air Electrodes with Ultrahigh Electrochemical Properties for Rechargeable Zinc–Air Batteries, *Adv. Funct. Mater.,* 2018, **28**, 1705048.

S15 Y. Xu, P. Deng, G. Chen, J. Chen, Y. Yan, K. Qi, H. Liu and B. Y. Xia, 2D Nitrogen-Doped Carbon Nanotubes/Graphene Hybrid as Bifunctional Oxygen Electrocatalyst for Long-Life Rechargeable Zn–Air Batteries, *Adv. Funct. Mater.,* 2019, **30**, 1906081.

S16 H. Guo, Q. Feng, J. Zhu, J. Xu, Q. Li, S. Liu, K. Xu, C. Zhang and T. Liu, Cobalt nanoparticle-embedded nitrogen-doped carbon/carbon nanotube frameworks derived from a metal–organic framework for tri-functional ORR, OER and HER electrocatalysis, *J. Mater. Chem. A,* 2019, **7**, 3664-3672.

S17 X. Wang, J. Sunarso, Q. Lu, Z. Zhou, J. Dai, D. Guan, W. Zhou and Z. Shao, High-Performance Platinum-Perovskite Composite Bifunctional Oxygen Electrocatalyst for Rechargeable Zn–Air Battery, *Adv. Energy Mater.,* 2019, **10**, 1903271.

S18 J. -S. Qin, D. -Y. Du, W. Guan, X. -J. Bo, Y. -F. Li, L. -P. Guo, Z. -M. Su, Y. -Y. Wang, Y. -Q. Lan and H. -C. Zhou, Ultrastable Polymolybdate-Based Metal–Organic Frameworks as Highly Active Electrocatalysts for Hydrogen Generation from Water, *J. Am. Chem. Soc.*, 2015, **137**, 7169-7177.

S19 T. Tian, L. Ai and J. Jiang, Metal–organic framework-derived nickel phosphides as efficient electrocatalysts toward sustainable hydrogen generation from water splitting, *RSC Adv.*, 2015, **5**, 10290-10295.

S20 J. -S. Li, B. Du, Z. -H. Lu, Q. -T. Meng and J. -Q. Sha, In situ-generated Co@nitrogen-doped carbon nanotubes derived from MOFs for efficient hydrogen evolution under both alkaline and acidic conditions, *New J. Chem.*, 2017, **41**, 10966-10971.

S21 Y. -P. Wu, W. Zhou, J. Zhao, W. -W. Dong, Y. -Q. Lan, D. -S. Li, C. Sun and X. Bu, Surfactant-Assisted Phase-Selective Synthesis of New Cobalt MOFs and Their Efficient Electrocatalytic Hydrogen Evolution Reaction, *Angew. Chem. Int. Ed.*, 2017, **56**, 13001-13005.

S22 R. Dong, Z. Zheng, D. C. Tranca, J. Zhang, N. Chandrasekhar, S. Liu, X. Zhuang, G. Seifert and X. Feng, Immobilizing Molecular Metal Dithiolene–Diamine Complexes on 2D Metal–Organic Frameworks for Electrocatalytic H2 Production, *Chem. Eur. J.*, 2017, **23**, 2255-2260.

S23 Y. Yang, Z. Lun, G. Xia, F. Zheng, M. He and Q. Chen, Non-precious alloy encapsulated in nitrogen-doped graphene layers derived from MOFs as an active and durable hydrogen evolution reaction catalyst, *Energy Environ. Sci.,* 2015, **8**, 3563-3571.

S24 L. Yan, P. Dai, Y. Wang, X. Gu, L. Li, L. Cao and X. Zhao, In Situ Synthesis Strategy for Hierarchically Porous Ni_2P Polyhedrons from MOFs Templates with Enhanced Electrochemical Properties for Hydrogen Evolution, *ACS Appl. Mater. Interfaces*, 2017, **9**, 11642-11650.

S25 L. Li, X. Li, L. Ai and J. Jiang, MOF-derived nanostructured cobalt phosphide assemblies for efficient hydrogen evolution reaction, *RSC Adv.*, 2015, **5**, 90265-90271.

S26 X. Li, L. Yang, T. Su, X. Wang, C. Sun and Z. Su, Graphene-coated hybrid electrocatalysts derived from bimetallic metal–organic frameworks for efficient hydrogen generation, *J. Mater. Chem. A*, 2017, **5**, 5000-5006.

S27 Y. Cheng, J. Guo, Y. Huang, Z. Liao and Z. Xiang, Ultrastable hydrogen evolution electrocatalyst derived from phosphide postmodified metal-organic frameworks, *Nano Energy*, 2017, **35**, 115-120.